Electronic Supplementary Material (ESI) for Journal of Materials Chemistry A.

Rational Constructing Macroporous CoFeP Triangular Plate Arrays from Bimetal-Organic Frameworks as High-Performance Overall Water-Splitting Catalysts

Ling Zhang; Xingyue Wang; Ang Li; Xingqun Zheng; Lishan Peng; Jiawei Huang; Zihua Deng; Hongmei Chen† and Zidong Wei†

The State Key Laboratory of Power Transmission Equipment & System Security and New Technology, Chongqing Key Laboratory of Chemical Process for Clean Energy and Resource Utilization, School of Chemistry and Chemical Engineering, Chongqing University, Shazhengjie 174, Chongqing 400044, China

* To whom correspondence should be addressed:

Email: chmcyj@cqu.edu.cn and zdwei@cqu.edu.cn

Materials Synthesis

Materials: Nickel foam was purchased from Kunshan Kuangxun Ltd. (China). Pt/C (40% Pt on Vulcan XC-72R) and RuO_2 were purchased from Sigma-Aldrich Chemical Reagent Co., Ltd., and 1,4-benzenedicarboxylic (BDC), KOH, NaOH, $CoCl_2 \cdot 6H_2O$, $FeCl_2$, $NaH_2PO_2 \cdot H_2O$, NH_4F from Shanghai Titan Science & Technology Co., Ltd. All reagents were used as received. The water used throughout all experiments was deionized water.

Synthesis of CoFe-MOF TPAs/Ni: CoFe-bimetal-organic framework were grown on nickel foam by a hydrothermal method (see Scheme 1). Take CoFe-MOF TPAs/Ni as an example. Firstly, 2.1 mmol of 1,4-benzenedicarboxylic (BDC) was dissolved in 35 ml water to form a turbid solution and then, the pH of the solution was kept at 8 by addition of 1 M NaOH with vigorous magnetic stirring for 15 min, referred to as Solution A. Secondly, 2.1 mmol of $CoCl_2 \cdot 6H_2O$, 2.1 mmol $FeCl_2$ and 8.4 mmol of NH_4F were dissolved in 35 ml water forming orange solution, referred to as Solution B. Subsequently, Solution A was mixed with Solution B under vigorous magnetic stirring until the solution turned transparent and yellow. The solution was then transferred into a 100 ml PTFE-lined stainless steel autoclave containing a piece of clean nickel foam (1×5 cm^2). The autoclave was sealed and heated at 120℃ for 6 h. Afterwards, the autoclave was cooled to room temperature and then its content was taken out and washed with ethanol and water in turn before being dried at 60℃ in air for 12 h (denoted as CoFe-MOF TPAs/Ni). With other experimental conditions fixed, maintaining the molar ratios of Co and Fe in Solution B at 1:0, 4:1, 3:2, 2:3, 1:4, 0:1, a series of samples (Co_xFe_y-MOF TPAs/Ni) were obtained. The actual Co/Fe atomic ratios in Co_xFe_y-MOF TPAs/Ni were determined by ICP-AES.

Fabrication of Macroporous CoFe-MOF TPAs/Ni: 70 ml of 30 mM NaOH was added into a 100 ml PTFE-lined stainless steel autoclave containing a piece of as-prepared CoFe-MOF TPAs/Ni. The autoclave was sealed and heated at 120℃ for 6 h. After the autoclave was cooled to room temperature, its content (denoted as Macroporous CoFe-MOF TPAs/Ni) was taken out and washed with ethanol and water in turn before being dried at 60℃ in air for 12 h. Fixing other hydrothermal reaction conditions, nanoplates with different pore sizes were achieved by changing the concentration of NaOH to 0, 10, 20, 30 and 40 mM and products denoted respectively as CoFe-MOF-0 TPAs/Ni, CoFe-MOF-10 TPAs/Ni, CoFe-MOF-20 TPAs/Ni, CoFe-MOF-30 TPAs/Ni and CoFe-MOF-40 TPAs/Ni. For convenience, the CoFe-MOF-30 TPAs/Ni also be denoted as Macroporous CoFe-MOF TPAs/Ni.

Preparation of Macroporous CoFeP TPAs/Ni: Phosphidation of as-prepared Macroporous CoFe-MOF TPAs/Ni was accomplished in a horizontal quartz tube furnace. Specifically, the Macroporous CoFe-MOF TPAs/Ni and $NaH_2PO_2 \cdot H_2O$ were put individually in two porcelain boats. The boat with $NaH_2PO_2 \cdot H_2O$ was placed at the upstream end of the furnace and the boat with Macroporous CoFe-MOF TPAs/Ni at the other end. The molar ratio of metal to P was 1:10. The furnace was heated to 350°C at a heating rate of 5℃ min^{-1} and maintained for 2 h in N_2 atmosphere (55 sccm). Then the reaction system was cooled naturally down to room temperature in the furnace to obtain Macroporous CoFeP TPAs/Ni. Fixing other condition, nanoplates with different pore sizes can also be obtained and denoted as CoFeP-0 TPAs/Ni, CoFeP-10 TPAs/Ni, CoFeP-20 TPAs/Ni, CoFeP-30 TPAs/Ni and CoFeP-40 TPAs/Ni.

Preparation of CoFeP/Ni: Preparation of CoFe-OH/Ni and its conversion into CoFeP/Ni were performed in similar procedures as CoFe-MOF TPAs/Ni and Macroporous CoFe-MOF TPAs/Ni respectively, except that, in the first step, the 1,4-benzenedicarboxylic anion (BDC) was replaced with hexamethylenetetramine (HMT).

Structural Characterization

Powder X-ray diffraction (PXRD) data were obtained using a PANalytical X'pert diffractometer with Cu Kα radiation (λ=1.5418 Å). The morphology and chemistry of the samples were characterized by a field emission scanning electron microscopy (FE-SEM) (model JSM-7600F, JEOL Ltd., Tokyo, Japan). Transmission electron microscopy (TEM) measurements were performed on a HITACHI H-8100 electron microscopy (Hitachi, Tokyo, Japan) with an accelerating voltage of 200 kV. The energy dispersive X-ray (EDX) mapping was carried out to

reveal the element composition and distribution in Macroporous CoFeP TPAs/Ni. X-ray photoelectron spectroscopy (XPS) measurements were conducted by using a Thermo ESCALAB 250Xi with an Al Kα (1486.6 eV) X-ray source on the samples with binding energies referenced to adventitious carbon at 284.8eV. UV-Vis absorption spectra were collected by an Agilent Cary 5000 UV-Vis-NIR Spectrophotometer. Nitrogen-adsorption and desorption isotherms was performed. The test was performed at 77 K using Kubo X1000 sorption analyzer instrument. The specific surface area of sample was estimated by Brunauer-Emmett-Teller (BET) method. The desorption branch of isotherms was used to calculate pore size distribution by Barrett-Joyner-Halenda (BJH) method. Inductively coupled plasma atomic emission spectrometry (ICP-AES) analysis was performed on ThermoScientific iCAP 6300 Duo.

Electrochemical characterization

The electrocatalytic properties of the prepared samples were evaluated with Autolab (Auto 72703) electrochemical workstation in a conventional three-electrode system. The Macroporous CoFeP TPAs/Ni, CoFeP/Ni, commercial Pt/C (40 wt % Pt/XC-72) on nickel foam and bare nickel foam were individually used as the working electrodes, a Hg/HgO electrode (1 M KOH) as the reference electrode, and a graphite plate as the counter electrode. The geometric surface area of the working electrode is 1.0×1.0 cm^2. The Hg/HgO reference electrode was calibrated with respect to RHE according to the previous study: in 1.0 M KOH, $E_{RHE} = E_{Hg/HgO} + 0.0591*pH+0.098$. Prior to recording the electroactivity, the catalysts were activated by 25 CV scans. Polarization curves were obtained using linear sweep voltammetry (LSV) conducted from 0.05 V to -0.7 V in 1.0 M KOH with a scan rate of 1 mV s^{-1} and chronopotentiometric measurements were carried out at different overpotentials. The electrochemical impedance spectroscopy (EIS) was carried out at an overpotential of 100 mV in a frequency range from 100 kHz to 0.01 Hz. The polarization curves were corrected against ohmic potential drop.

Electrochemical active surface area

Cyclic voltammetry was used to measure the electrochemically active surface area (ECSA) in the non-Faraday range of 0.1- 0.2 V vs. RHE with different scan rates of 8, 11, 14, 17, 20, 23, 26, 29, 32 and 35 mV s^{-1}. Plotting the current density ($j=(j_a-j_c)/2$) at 0.15 V against the scan rate, the linear slope (= 311.8 mF) is the double layer capacitance (C_{dl}). The ECSA was calculated by dividing double-layer capacitance (C_{dl}) by the specific capacitance (C_s=40 μF cm^{-2}) of flat electrodes in 1 M KOH[1-3].

$$A_{ECSA} = \frac{C_{dl}}{C_s} = \frac{311.8\text{mF}}{40\mu\text{F cm}^{-2}} = 7795 \text{ cm}^{-2}$$

The LSV curves were normalized by ECSA according to the following formula[1].

$$J_{ECSA} = \frac{J}{A_{ECSA}}$$

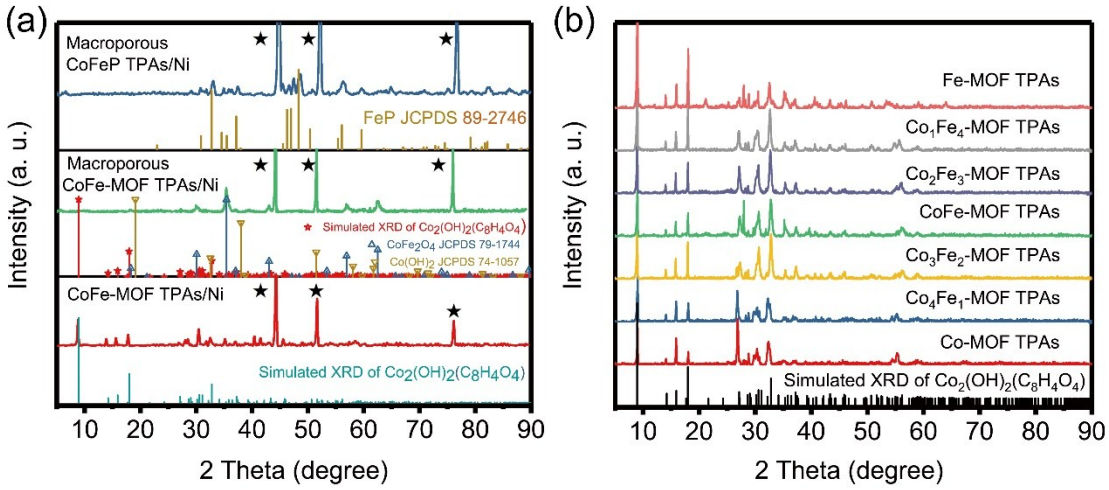

Figure S1 XRD patterns of CoFe-MOF TPAs/Ni, Macroporous CoFe-MOF TPAs/Ni and Macroporous CoFeP TPAs/Ni (a) and Co_xFe_y-MOF TPAs (b) powder scrape from nickel substrate

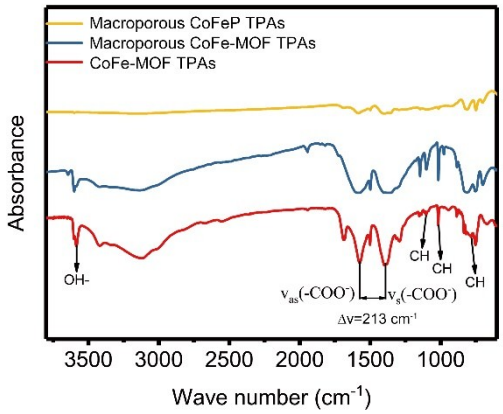

Figure S2 FTIR of CoFe-MOF TPAs, Macroporous CoFe-MOF TPAs and Macroporous CoFeP TPAs

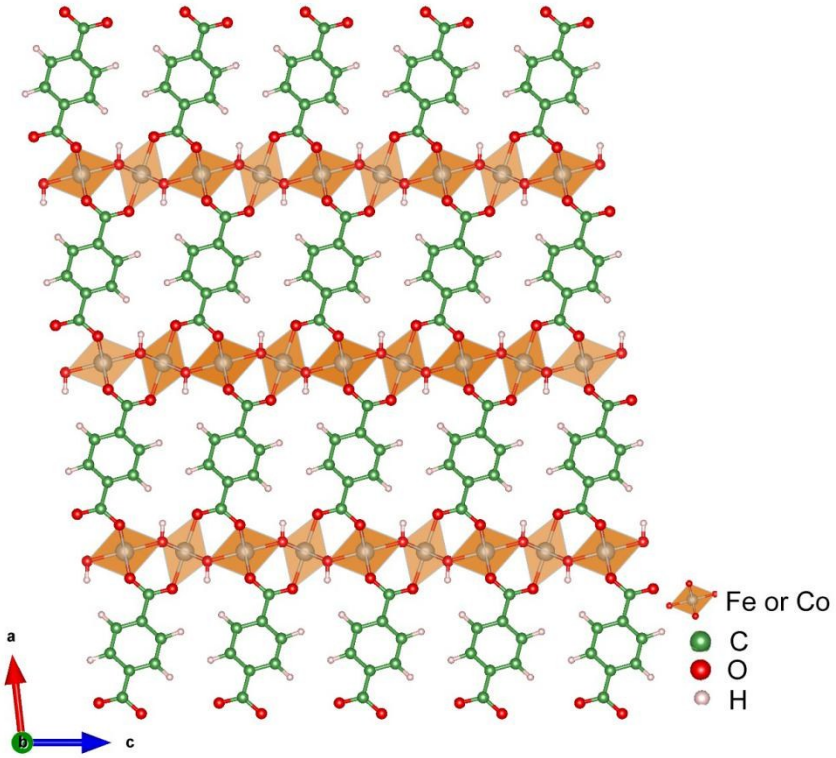

Figure S3 Crystal structure of CoFe-MOF.

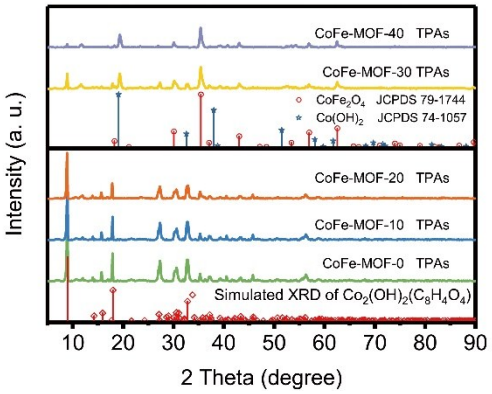

Figure S4 XRD patterns of CoFe-MOF-0 TPAs, CoFe-MOF-10 TPAs, CoFe-MOF-20 TPAs, CoFe-MOF-30 TPAs, CoFe-MOF-40 TPAs powder scrape from nickel substrate

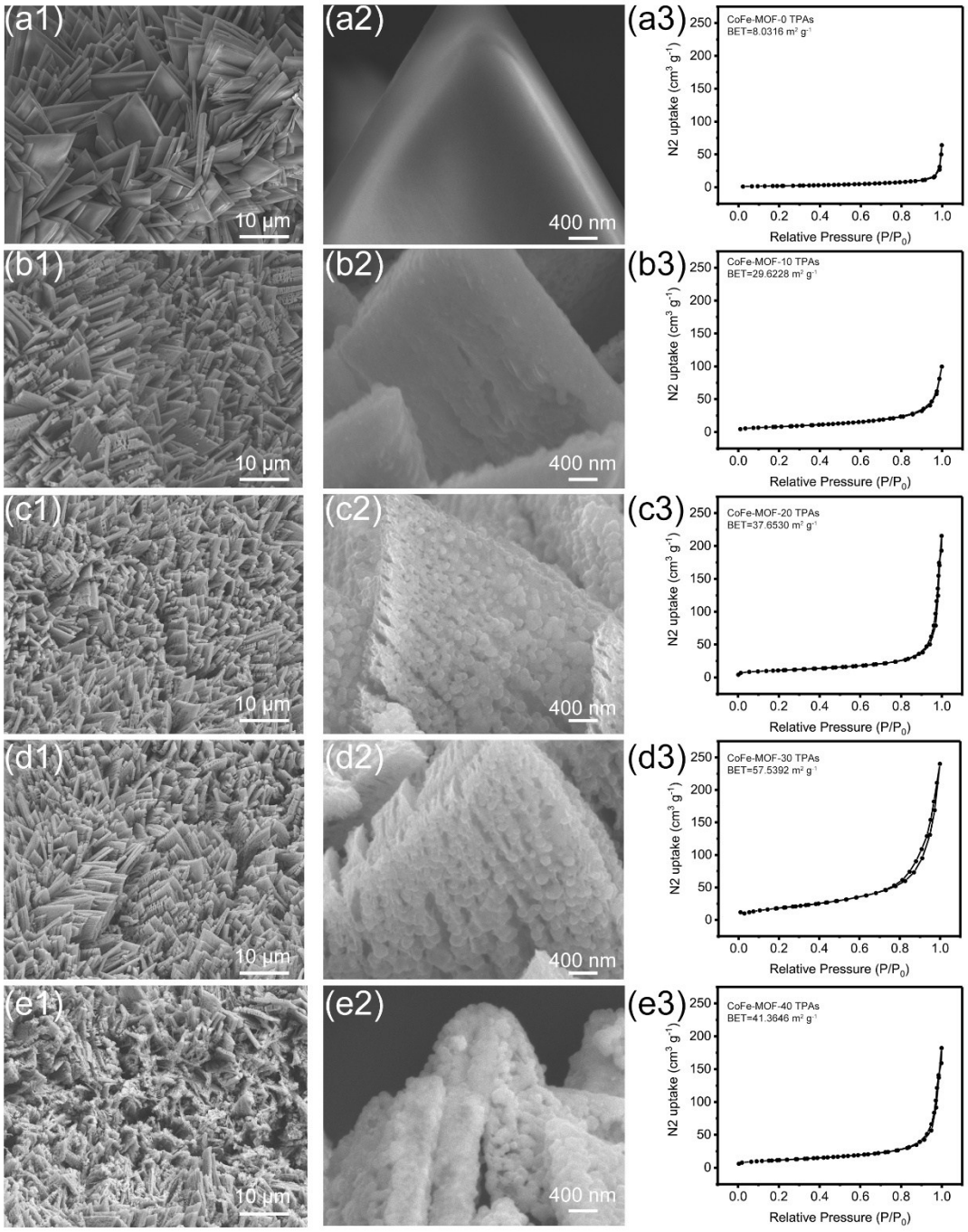

Figure S5 SEM of pristine and NaOH etched precursors and corresponding N_2 sorption isotherms: (a1~ a3) CoFe-MOF-0 TPAs/Ni; (b1~ b3) CoFe-MOF-10 TPAs/Ni; (c1~ c3) CoFe-MOF-20 TPAs/Ni; (d1~ d3) CoFe-MOF-30 TPAs/Ni; (e1~ e3) CoFe-MOF-40 TPAs.

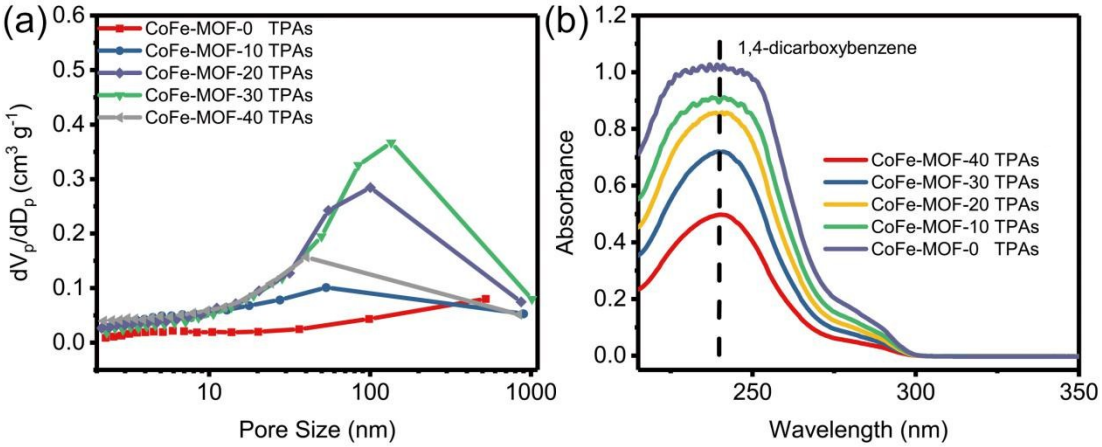

Figure S6 Pore distribution profiles (a) and Uv-vis (b) of CoFe-MOF TPAs, CoFe-MOF-10 TPAs, CoFe-MOF-20 TPAs, Macroporous CoFe-MOF TPAs and CoFe-MOF-40 TPAs.

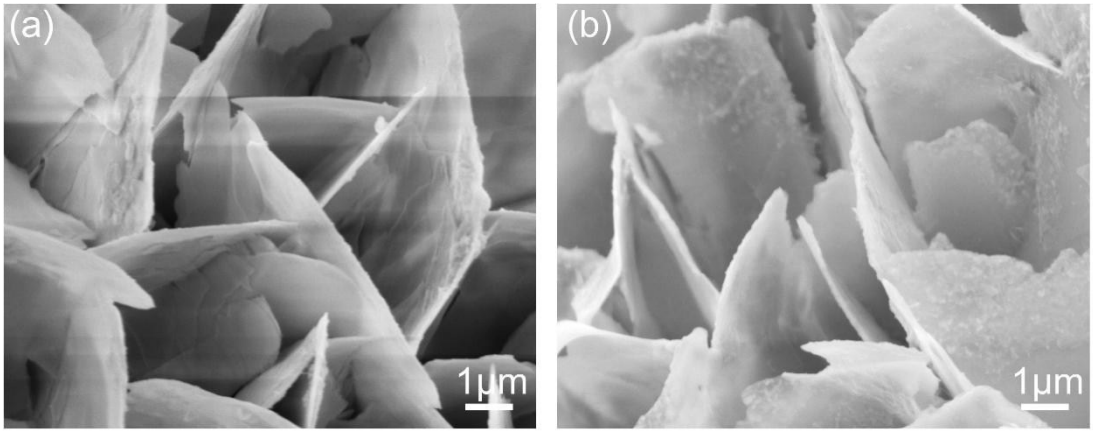

Figure S7 SEM images of CoFe-OH/Ni before (a) and after 30 mM NaOH treatment (b)

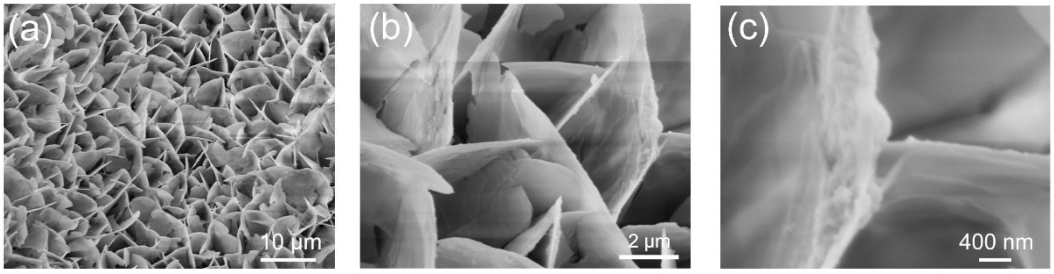

Figure S8 SEM images of CoFeP/Ni

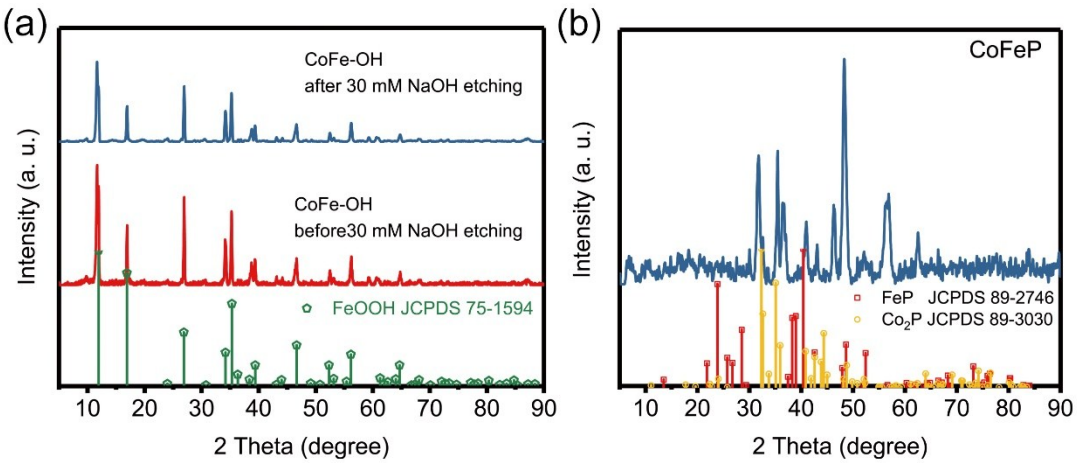

Figure S9 (a) XRD patterns of CoFe-OH powder scrape from nickel substrate before and after NaOH etching; (b) XRD pattern of CoFeP powder scrape from nickel substrate

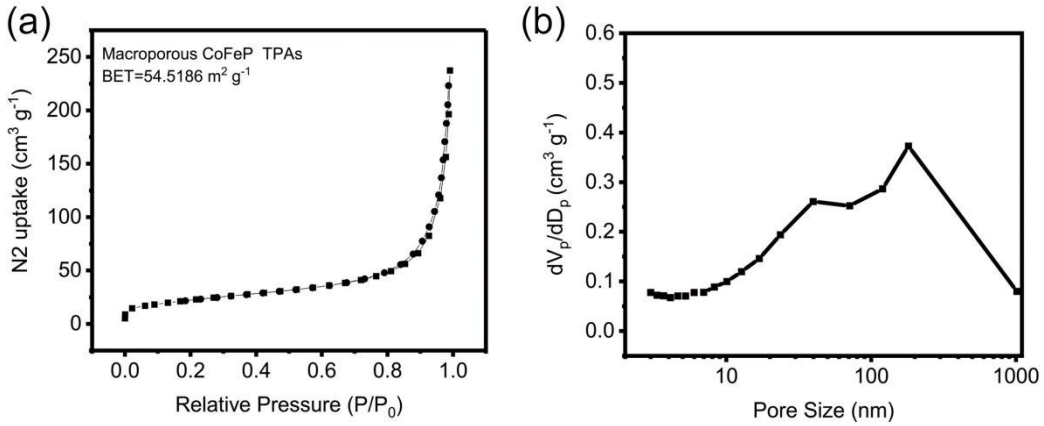

Figure S10 N_2 sorption isotherms (a) and pore distribution profiles (b) for Macroporous CoFeP TPAs

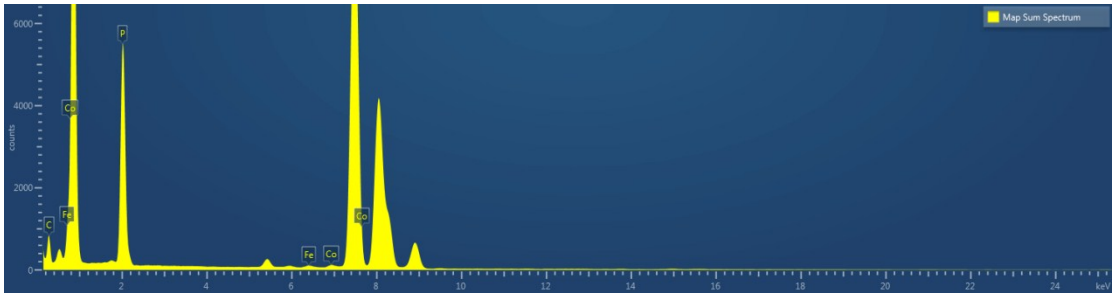

Figure S11 EDS pattern of the Macroporous CoFeP TPAs

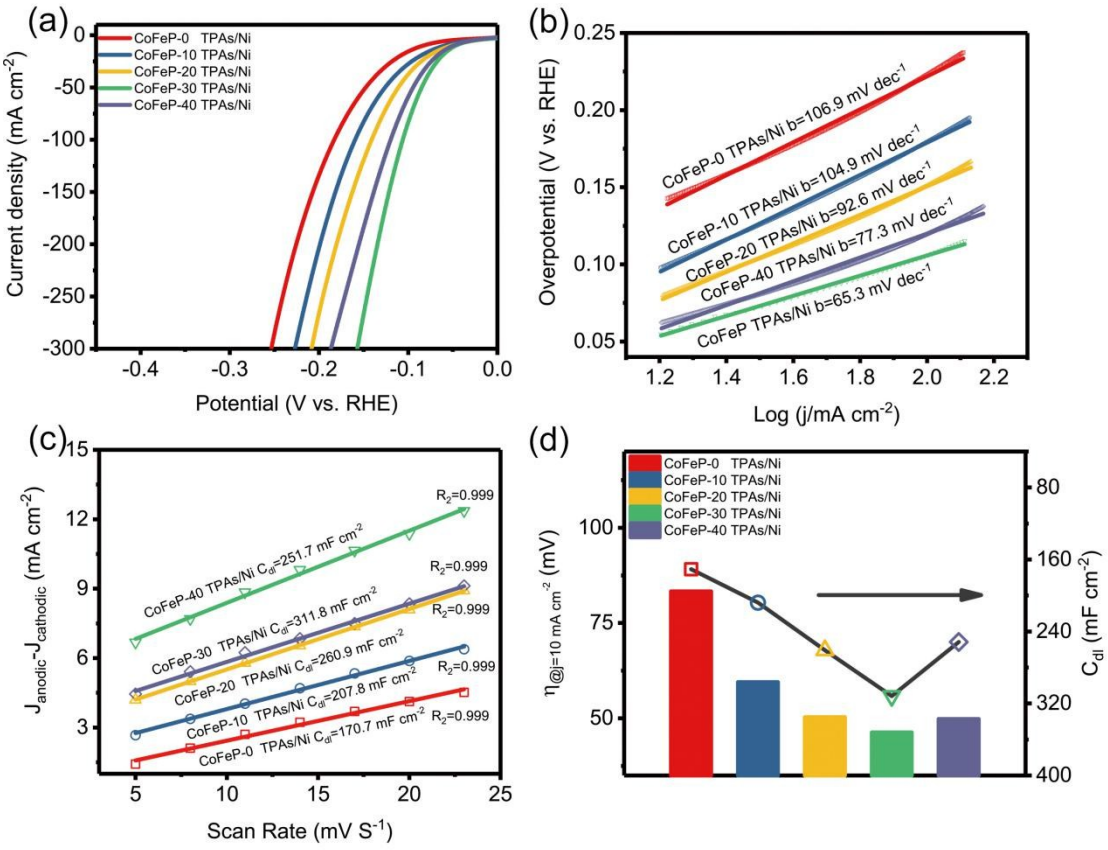

Figure S12 (a) LSV curves, (b) Corresponding Tafel slopes and (c) Capacitive current densities as a function of scan rate of pristine and CoFeP TPAs/Ni etched with different NaOH concentrations; (d) Overpotentials versus RHE at 10 mA cm^{-2} (left) and C_{dl} (right).

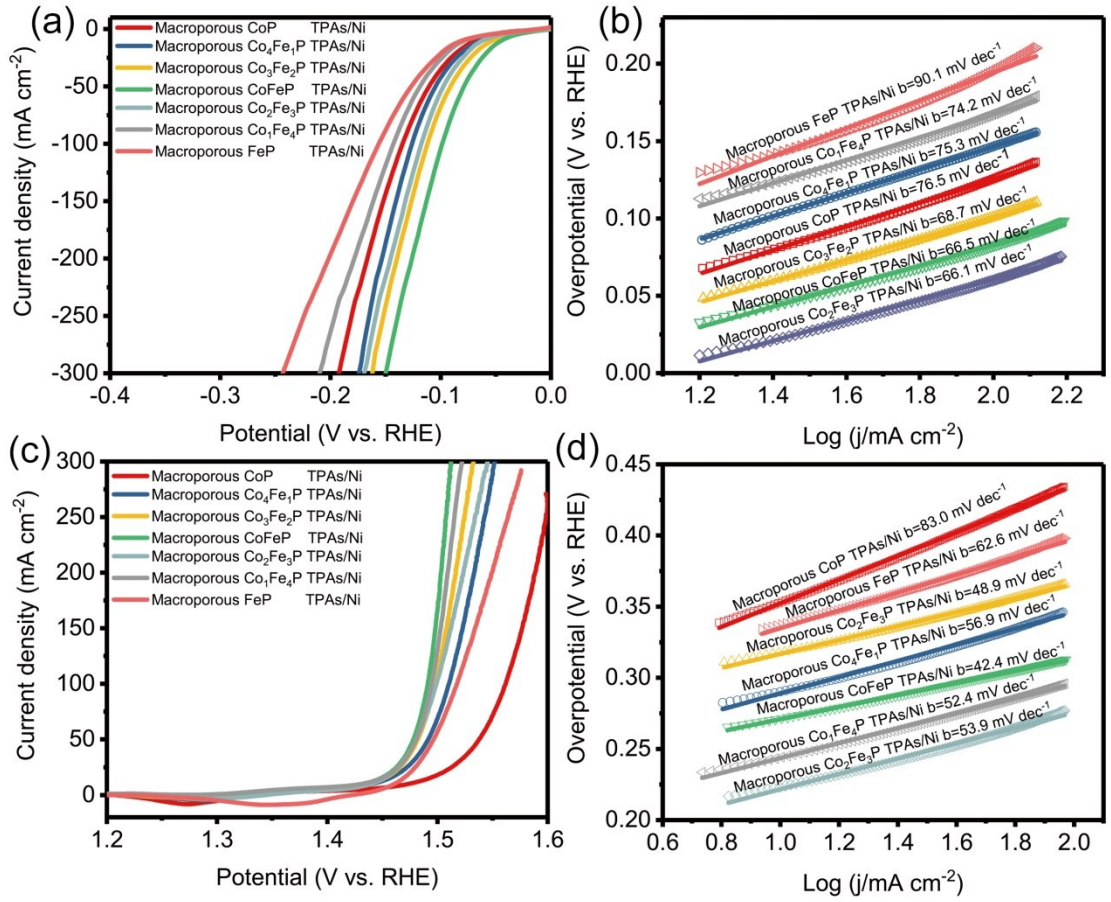

Figure S13 (a) LSV curves and (b) Corresponding Tafel slopes of Macroporous Co_xFe_yP TPAs/Ni (x:y=1:0, 4:1, 3:2, 1:1, 2:3, 1:4, 0:1) in 1 M KOH with a scan rate of 1 mV s^{-1}; (c) LSV curves and (d) Corresponding Tafel slopes of Macroporous Co_xFe_yP TPAs/Ni and Macroporous CoFeP TPAs/Ni in 1 M KOH with a scan rate of 1 mV s^{-1}.

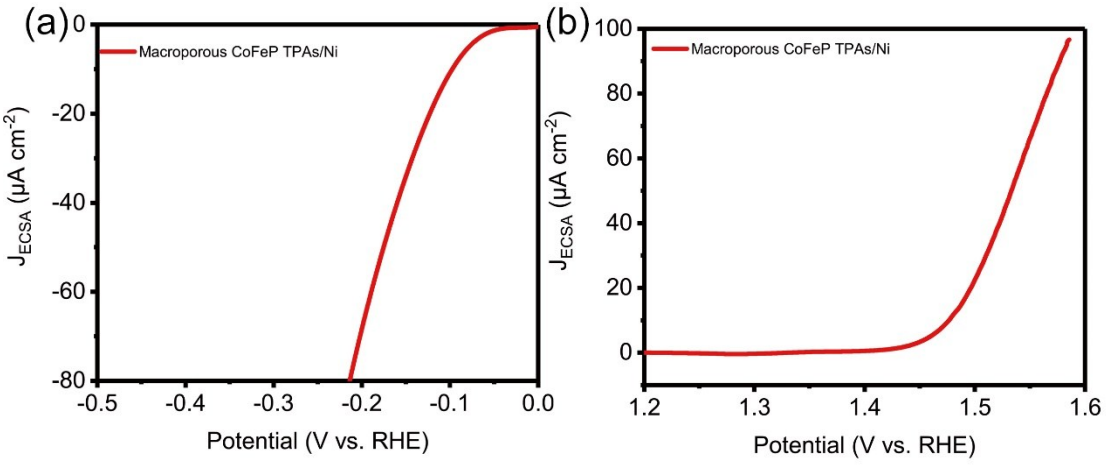

Figure S14 LSV curves normalized by ECSA for HER (a) and OER (b)

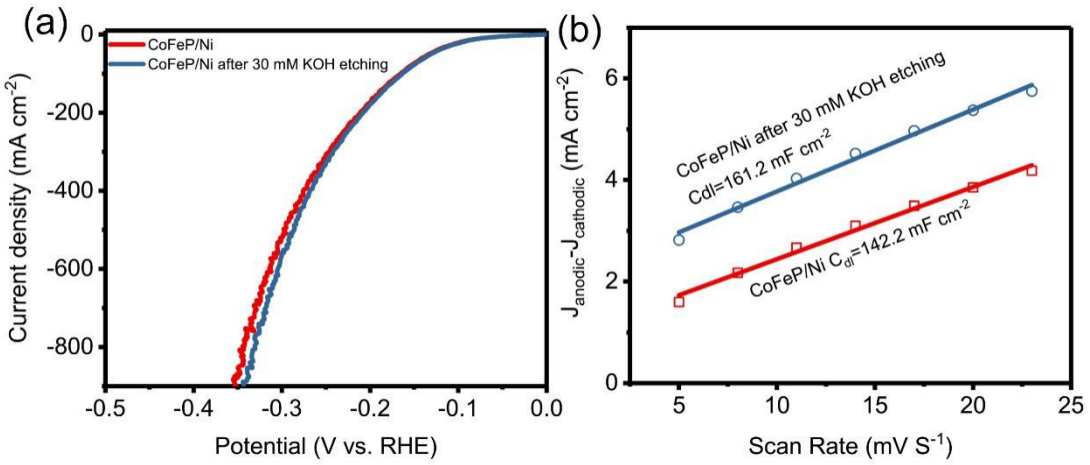

Figure S15 (a) LSV curves for CoFeP/Ni before and after 30 mM NaOH etching; (b) C_{dl} for CoFeP/Ni before and after 30 mM NaOH etching

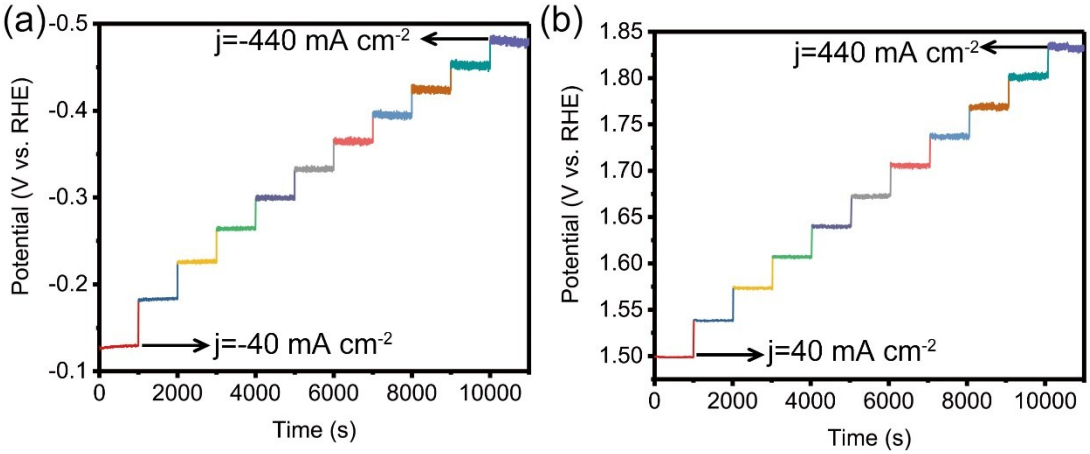

Figure S16 Chronoamperometric curves of Macroporous CoFeP TPAs/Ni in 1 M KOH (without iR) for HER (a) and OER (b)

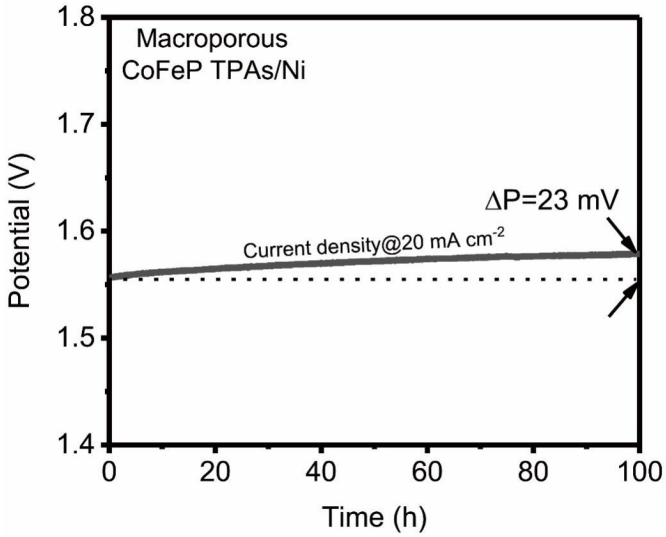

Figure S17 Chronopotentiometric curve of water electrolysis by Macroporous CoFeP TPAs/Ni in a two-electrode configuration with a constant current density of 20 mA cm^{-2}

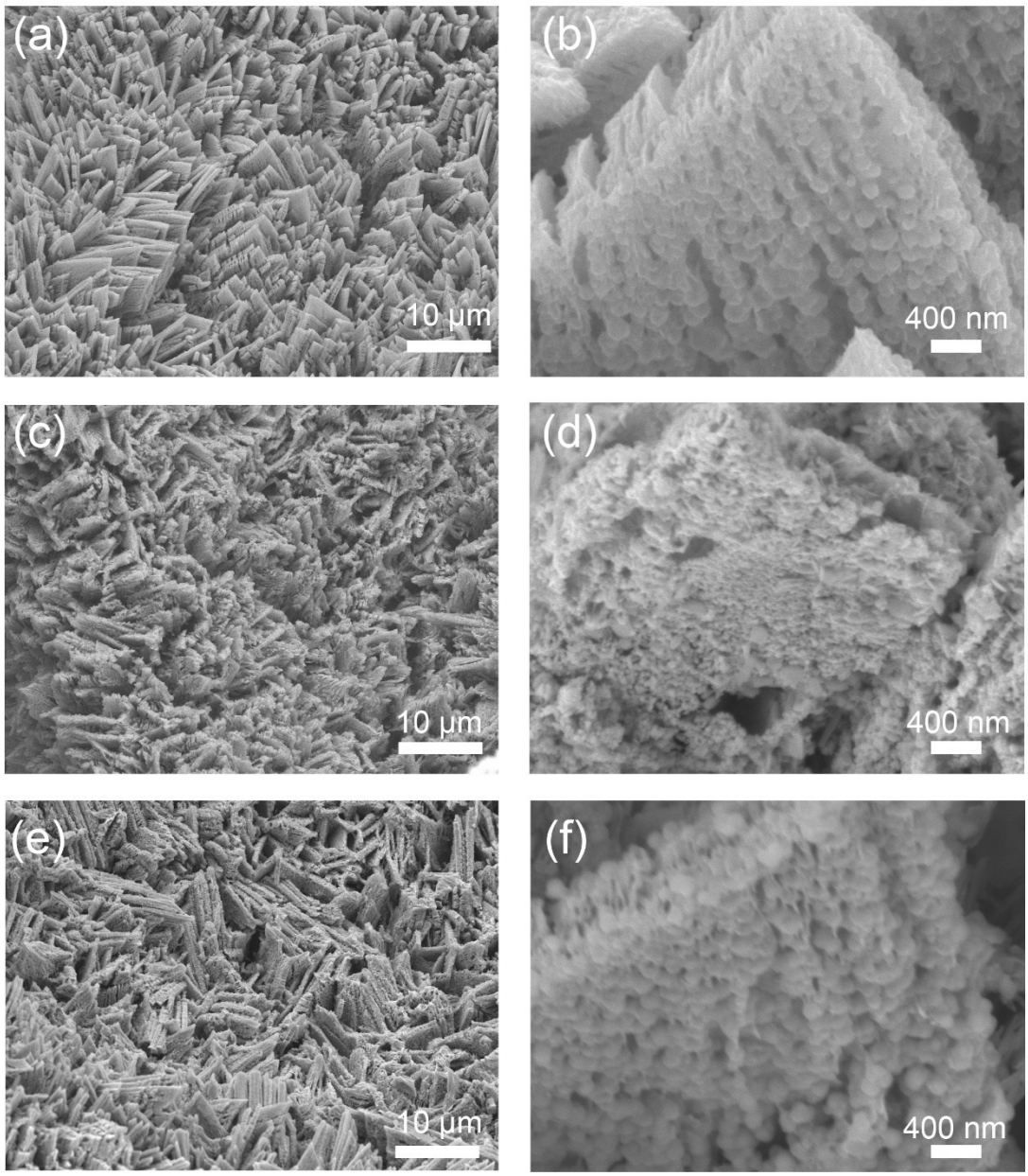

Figure S18 (a, b) SEM images of Macroporous CoFeP TPAs/Ni before and after 100 h of stability test at a constant current density for HER (c, d) and OER (e, f), respectively.

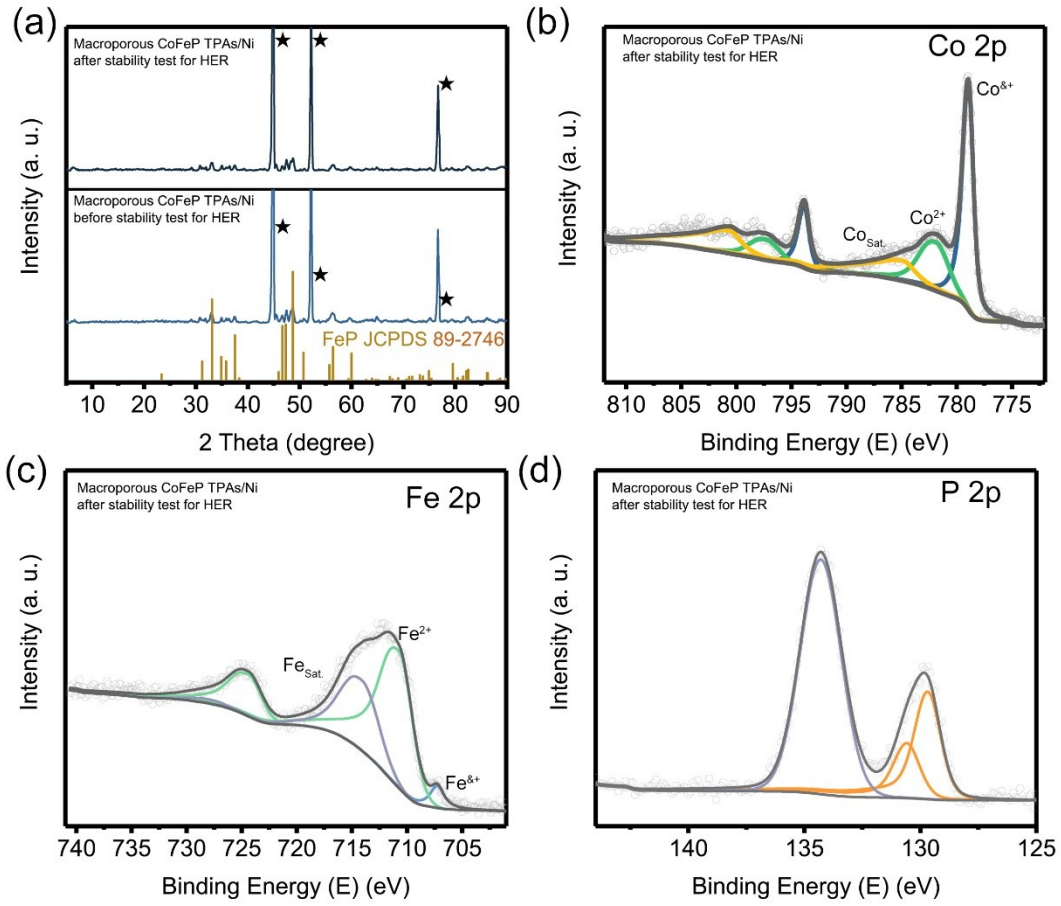

Figure S19 (a) XRD patterns of Macroporous CoFeP TPAs/Ni before and after stability test for HER; (b, c, d) High resolution XPS spectra of Macroporous CoFeP TPAs/Ni after stability test for HER.

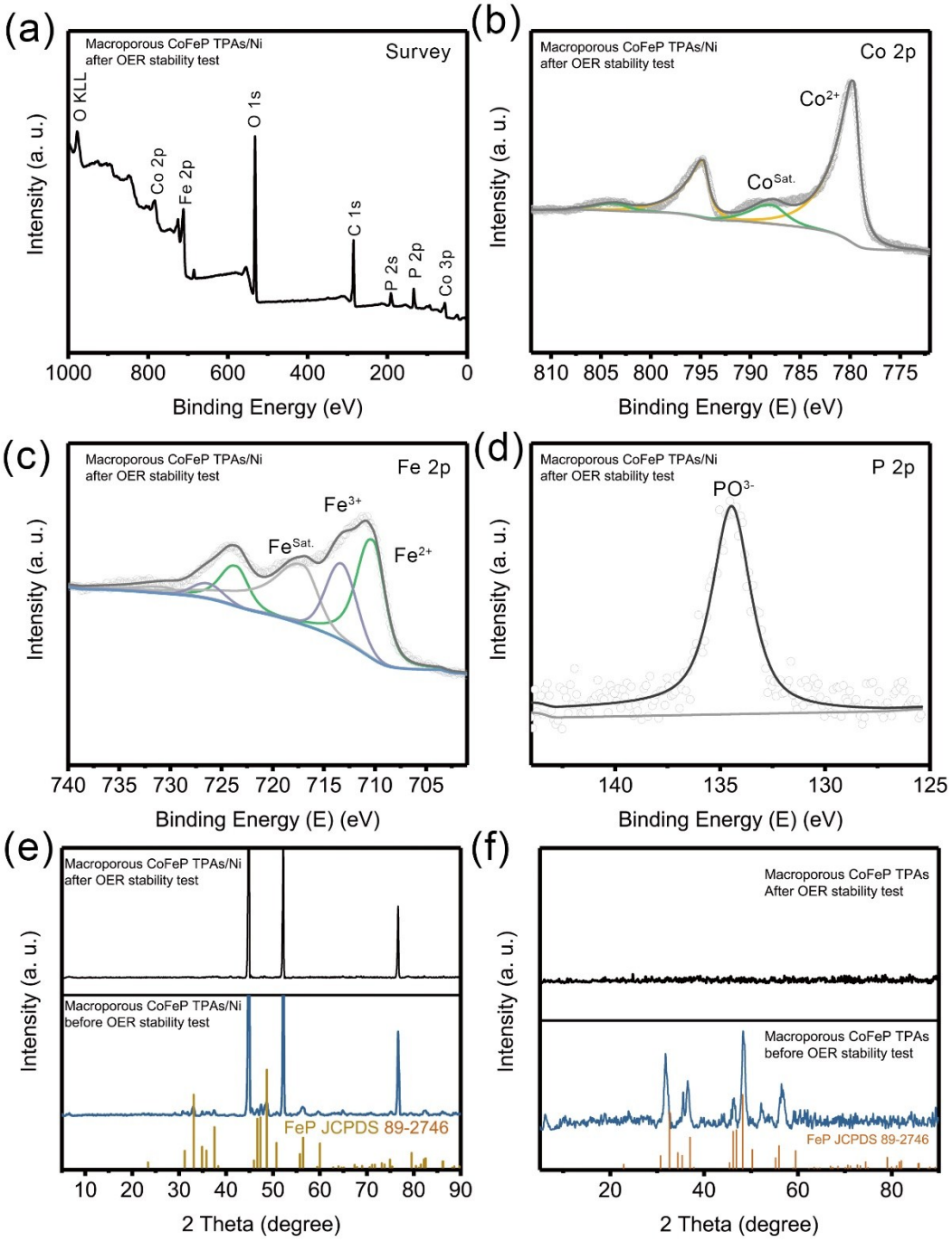

Figure S20 (a~d) XPS spectra of Macroporous CoFeP TPAs/Ni after stability test for OER; XRD patterns of (e) the Macroporous CoFeP TPAs/Ni on nickel foam directly and (f) the Macroporous CoFeP TPAs powder scrape from nickel substrate

Table S1 ICP-AES data for Co_xFe_y-MOF TPAs/Ni and their corresponding phosphides

Samples	Co(μg/ml)	Fe(μg/ml)	Co:Fe molar ratio
Fe-MOF TPAs/Ni	0	13.97	0:1
Co_1Fe_4-MOF TPAs/Ni	1.495	10.55	1:7
Co_2Fe_3-MOF TPAs/Ni	3.859	11.58	1:3
CoFe-MOF TPAs/Ni	4.018	8.035	1:2
Co_3Fe_2-MOF TPAs/Ni	8.526	9.527	6:7
Co_4Fe_1-MOF TPAs/Ni	8.071	3.528	13:6
Co-MOF TPAs/Ni	3.544	0	1:0
Macroporous CoFe-MOF TPAs/Ni	2.872	5.916	1:2
Macroporous FeP TPAs/Ni	0	11.23	0:1
Macroporous Co_1Fe_4P TPAs/Ni	1.034	7.290	1:7
Macroporous Co_2Fe_3P TPAs/Ni	2.854	8.819	1:3
Macroporous CoFeP TPAs/Ni	3.564	7.235	1:2
Macroporous Co_3Fe_2P TPAs/Ni	4.762	5.801	6:7
Macroporous Co_4Fe_1P TPAs/Ni	6.325	5.124	13:6
Macroporous CoP TPAs/Ni	8.756	0	1:0

Table S2. Summary of HER activities of Macroporous CoFeP TPAs/Ni, CoFeP/Ni, nickel substrate and 40% Pt/C on the nickel foam.

Samples	$\eta_{10\ mA\ cm^{-2}}$ (mV)	$\eta_{300\ mA\ cm^{-2}}$ (mV)	$\eta_{900\ mA\ cm^{-2}}$ (mV)	Tafel slope (mV dec^{-1})	$j_{0,\ geometric}$ (mA cm^{-2})	C_{dl} (mF cm^{-2})	Relative surface area
Macroporous CoFeP TPAs/Ni	43	153	263	65.3	2.40	311.8	173
CoFeP/Ni	76	230	322	96.7	1.94	142.2	79
nickel substrate	263	\	\	158.5	0.32	1.8	1
40% Pt/C	19	217	\	37.2	4.58	\	\

Table S3 Summary of OER activities of Macroporous CoFeP TPAs/Ni, CoFeP/Ni, nickel substrate and RuO_2 on the nickel foam

Samples	$\eta_{10\ mA\ cm^{-2}}$ (mV)	$\eta_{300\ mA\ cm^{-2}}$ (mV)	$\eta_{700\ mA\ cm^{-2}}$ (mV)	Tafel slope (mV dec^{-1})	$j_{0,\ geometric}$ (mA cm^{-2})
Macroporous CoFeP TPAs/Ni	198	290	335	42.0	0.000106
CoFeP/Ni	210	310	400	48.9	0.00028
nickel substrate	300	\	\	61.9	0.000124
RuO_2	230	380	460	80.7	0.0139

Table S4 Comparison of HER performance of Macroporous CoFeP TPAs/Ni and other non-precious metal HER catalysts in 1 M KOH

Catalysis	ŋ at 10 mA cm^{-2} (mV)	Tafel slope (mV dec^{-1})	Ref
Macroporous CoFeP TPAs/Ni	43@10 mA cm^{-2}	65.3	This work
	153@300 mA cm^{-2}		
	263@900 mA cm^{-2}		
NF@Ni/C-600	37	57	4
Fe-CoP HTPAs	98	69	5
$(Co, Ni)_2P$@0.1TiO_2	92	49	6
NiMoO C-30	76	78	7
Cu NDs/Ni_3S_2 NTs-CFs	128	76.2	8
PANI/CoP HNWs-CFs	50	34.5	9
FeCoP UNSAs	188@100 mA cm^{-2}	76	10
Ni@Ni_2P-Ru	51	41	11
CoP/Ni_5P_4/CoP	71	58	12
$Fe_{1.89}Mo_{4.11}O_7/MoO_2$	197	79	13
Ni–Co–P HNBs	107	46	14
H-NiCoP NWAs/NF	44	38.6	15
MoP/CNT	83	72	16
$Co_{2.90}B_{0.73}P_{0.27}$	42	42.1	17
Cu_3P	130	83	18
$NiCoSe_2$/CC	76.7	65	19
Ni_2P–NiP_2 HTPAs/NF	59.7	58.8	20
$MoS_2/Fe_5Ni_4S_8$	120	61.8	21
IrP_2@NC	28	50	22
CoP-Co_2P@PC/PG NHs	39	59	23
Ni-doped FeP/C hollow nanorods	95	72	24
porous $Co_{0.75}Ni_{0.25}(OH)_2$ nanosheets	95	85	25
CTGU-10c2	240	58	26
$Ni_{0.8}Co_{0.1}Fe_{0.1}O_xH_y$	85	84.5	27
Fe17.5%-Ni_3S_2/NF	47	95	28
R-NCO	90	52	29
CoMnP/Ni_2P/NiFe	87	95	30
Pt-αFe_2O_3	90	50.6	31
$FePSe_3$	118	88	32
Co/Co_2P@ACF/CNT	78	49	33
$(Fe_xNi_{1-x})_2P$	103	76.6	34
MoNiNC/Ni	110	118	35
CoNC@MoS_2/CNF	143	68	36

Table S5 Comparison of OER performance of Macroporous CoFeP TPAs/Ni and other non-precious metal HER catalysts in 1 M KOH

Catalysis	ŋ at 10 mA cm^{-2}	Tafel slope ($mV\ dec^{-1}$)	Ref
Macroporous CoFeP TPAs/Ni	198@10 mA cm^{-2}	42.0	This work
	290@300 mA cm^{-2}		
	335@700 mA cm^{-2}		
NF@Ni/C-600	265	54	4
Fe-CoP HTPAs	230	43	5
CoNi(20:1)-P-NS	273	45	37
FeCoP UNSAs	330@100 mA cm^{-2}	63	10
Ni–Co–P HNBs	270	76	14
Cu_3P	290	77	18
$NiCoSe_2$/CC	255.8	71	19
h-PNRO/C	239	52	38
$MoS_2/Fe_5Ni_4S_8$	204	28.1	21
$Co_{1.75}Al_{1.25}O_4$	248	80.6	39
porous $Co_{0.75}Ni_{0.25}(OH)_2$ nanosheets	235	56	25
Co/CNFs(1000)	320	79	40
NF@NC-$CoFe_2O_4$/C NRAs	240	45	41
$Ni_{0.8}Co_{0.1}Fe_{0.1}O_xH_y$	239	45.4	27
Fe17.5%-Ni_3S_2/NF	214	42	28
R-NCO	260	50	29
CoMnP/Ni_2P/NiFe	204	60	30
Pt-αFe_2O_3	304@50	50.3	31
VO_x/Ni_3S_2@NF	358@100	82	42
Fe-CoP/CoO	219	52	43
$Co_xFe_{1-x}WO_4$	327	53	44
hollow Ru-RuP_x-Co_xP	291	85.4	45
Co-MnO_2|OV	297	75	46
E-CoO_x/CF	249	50	47
Fe-doped $NiPS_3$	256@30	46	48
S–FeNi@NC	272@20	84	49
PIZA-1	340	47.6	50
NiCo-UMOFNs	250	65	51
hollow CoS_2	276	81	52
NiCoP/NC PHCs	297	51	53
NiFe-MOF array	240	34	54
CoNC@MoS_2/CNF	257	51.9	36

Table S6 Comparison of water splitting performance of Macroporous CoFeP TPAs/Ni and other non-precious metal HER catalysts in 1 M KOH

Catalysis	ŋ at 10 mA cm^{-2} （V）	Ref
Macroporous CoFeP TPAs/Ni	1.47@10 mA cm^{-2}	This work
	1.81@100 mA cm^{-2}	
	1.70@100 mA cm^{-2} (60°C)	
NF@Ni/C-600	35.9@1.60	4
NiFe LDH/NF	1.7	55
Fe-CoP HTPAs	1.59	5
NiSe/NF	1.63	56
FeCoP UNSAs	1.6	10
Ni–Co–P HNBs	1.62	14
CoP-Co_2P@PC/PG NHs	1.57	23
CoS-$Co(OH)_2$@MoS_{2+x}/NF	1.58	57
porous $Co_{0.75}Ni_{0.25}(OH)_2$ nanosheets	1.56	25
$Ni_{0.8}Co_{0.1}Fe_{0.1}O_xH_y$	1.58	27
Ni/Ni_8P_3	1.61	58
MoS_2/Ni_3S_2	1.56	59
Fe-Ni_3S_2/NF	1.54	28
R-NCO	1.61	29
CoMnP/Ni_2P/NiFe	1.48	30
Pt-αFe_2O_3	1.51	31
hollow CoS_2	1.61	52
CoNC@MoS_2/CNF	1.62	36
$MoNi_4$/MoO_{3-x}//NiFe-LDH	1.53	60
NiCoP	1.58	61

Reference

1 J. Kibsgaard, C. Tsai, K. Chan, J. D. Benck, J. K. Nørskov, F. Abild-Pedersen and T. F. Jaramillo, *Energ. Environ. Sci.,* 2015, **8**, 3022-3029.
2 J. Kibsgaard and T. F. Jaramillo, *Angew. Chem. Int. Edit.,* 2014, **53**, 14433-14437.
3 R. Zhang, X. Wang, S. Yu, T. Wen, X. Zhu, F. Yang, X. Sun, X. Wang and W. Hu, *Adv. Mater.,* 2017, **29**, 1605502.
4 H. Sun, Y. Lian, C. Yang, L. Xiong, P. Qi, Q. Mu, X. Zhao, J. Guo, Z. Deng and Y. Peng, *Energ. Environ. Sci.,* 2018, **11**, 2363-2371.
5 E. Hu, J. Ning, D. Zhao, C. Xu, Y. Lin, Y. Zhong, Z. Zhang, Y. Wang and Y. Hu, *Small*, 2018, **14**, 1704233.
6 X. Liu, Q. Hu, B. Zhu, G. Li, L. Fan, X. Chai, Q. Zhang, J. Liu and C. He, *Small*, 2018, **14**, 1802755.
7 Y. Zhang, B. Ouyang, K. Xu, X. Xia, Z. Zhang, R. S. Rawat and H. J. Fan, *Small*, 2018, **14**, 1800340.
8 J. X. Feng, J. Q. Wu, Y. X. Tong and G. R. Li, *J. Am. Chem. Soc.,* 2018, **140**, 610-617.
9 J. X. Feng, S. Y. Tong, Y. X. Tong and G. R. Li, *J. Am. Chem. Soc.,* 2018, **140**, 5118-5126.
10 L. Zhou, M. Shao, J. Li, S. Jiang, M. Wei and X. Duan, *Nano Energy*, 2017, **41**, 583-590.
11 Y. Liu, S. Liu, Y. Wang, Q. Zhang, L. Gu, S. Zhao, D. Xu, Y. Li, J. Bao and Z. Dai, *J. Am. Chem. Soc.,* 2018, **140**, 2731-2734.
12 K. Mishra, H. Zhou, J. Sun, F. Qin, K. Dahal, J. Bao, S. Chen and Z. Ren, *Energ. Environ. Sci.,* 2018, **11**, 2246-2252.
13 Z. Hao, S. Yang, J. Niu, Z. Fang, L. Liu, Q. Dong, S. Song and Y. Zhao, *Chem. Sci.,* 2018, **9**, 5640-5645.
14 E. Hu, Y. Feng, J. Nai, D. Zhao, Y. Hu and X. W. Lou, *Energ. Environ. Sci.,* 2018, **11**, 872-880.
15 C. Liu, G. Zhang, L. Yu, J. Qu and H. Liu, *Small*, 2018, **14**, 1800421.
16 X. Zhang, X. Yu, L. Zhang, F. Zhou, Y. Liang and R. Wang, *Adv. Funct. Mater.,* 2018, **28**, 1706523.
17 H. Sun, X. Xu, Z. Yan, X. Chen, L. Jiao, F. Cheng and J. Chen, *J. Mater. Chem. A*, 2018, **6**, 22062-22069.
18 J. Hao, W. Yang, Z. Huang and C. Zhang, *Adv. Mater. Interfaces*, 2016, **3**, 1600236.
19 J. Yu, Y. Tian, F. Zhou, M. Zhang, R. Chen, Q. Liu, J. Liu, C.-Y. Xu and J. Wang, *J. Mater. Chem. A*, 2018, **6**, 17353-17360.
20 T. Liu, A. Li, C. Wang, W. Zhou, S. Liu and L. Guo, *Adv. Mater.,* 2018, **30**, 1803590.
21 Y. Wu, F. Li, W. Chen, Q. Xiang, Y. Ma, H. Zhu, P. Tao, C. Song, W. Shang, T. Deng and J. Wu, *Adv. Mater.,* 2018, **30**, 1803151.
22 Z. Pu, J. Zhao, I. S. Amiinu, W. Li, M. Wang, D. He and S. Mu, *Energ. Environ. Sci.,* 2019, **12**, 952-957.
23 J. Yang, D. Guo, S. Zhao, Y. Lin, R. Yang, D. Xu, N. Shi, X. Zhang, L. Lu, Y. Q. Lan, J. Bao and M. Han, *Small*, 2019, **15**, 1804546.
24 X. F. Lu, L. Yu and X. W. D. Lou, *Sci. Adv.,* 2019, **5**, eaav6009.
25 X. Wang, Z. Li, D. Y. Wu, G. R. Shen, C. Zou, Y. Feng, H. Liu, C. K. Dong and X. W. Du, *Small*, 2019, **15**, 1804832.
26 W. Zhou, D. D. Huang, Y. P. Wu, J. Zhao, T. Wu, J. Zhang, D. S. Li, C. Sun, P. Feng and X. Bu, *Angew. Chem. Int. Edit.,* 2019, **58**, 4227-4231.
27 Q. Zhao, J. Yang, M. Liu, R. Wang, G. Zhang, H. Wang, H. Tang, C. Liu, Z. Mei, H. Chen and F. Pan, *ACS Catal.,* 2018, **8**, 5621-5629.
28 G. Zhang, Y.-S. Feng, W.-T. Lu, D. He, C.-Y. Wang, Y.-K. Li, X.-Y. Wang and F.-F. Cao, *ACS Catal.,* 2018, **8**, 5431-5441.
29 S. Peng, F. Gong, L. Li, D. Yu, D. Ji, T. Zhang, Z. Hu, Z. Zhang, S. Chou, Y. Du and S. Ramakrishna, *J. Am. Chem. Soc.,* 2018, **140**, 13644-13653.
30 X. Bu, R. Wei, W. Gao, C. Lan and J. C. Ho, *J. Mater. Chem. A*, 2019, **7**, 12325-12332.
31 B. Ye, L. Huang, Y. Hou, R. Jiang, L. Sun, Z. Yu, B. Zhang, Y. Huang and Y. Zhang, *J. Mater. Chem. A*, 2019, **7**, 11379-11386
32 J. Yu, W.-J. Li, H. Zhang, F. Zhou, R. Li, C.-Y. Xu, L. Zhou, H. Zhong and J. Wang, *Nano Energy*, 2019, **57**, 222-229.
33 F. Wang, L. Hu, R. Liu, H. Yang, T. Xiong, Y. Mao, M. S. Balogun, G. Ouyang and Y. Tong, *J. Mater. Chem. A*, 2019,**7**, 11150-11159
34 W. Zhang, Y. Zou, H. Liu, S. Chen, X. Wang, H. Zhang, X. She and D. Yang, *Nano Energy*, 2019, **56**, 813-822.
35 F. Wang, Y. Sun, Y. He, L. Liu, J. Xu, X. Zhao, G. Yin, L. Zhang, S. Li, Q. Mao, Y. Huang, T. Zhang and B. Liu, *Nano Energy*, 2017, **37**, 1-6.
36 D. Ji, S. Peng, L. Fan, L. Li, X. Qin and S. Ramakrishna, *J. Mater. Chem. A*, 2017, **5**, 23898-23908.
37 X. Xiao, C.-T. He, S. Zhao, J. Li, W. Lin, Z. Yuan, Q. Zhang, S. Wang, L. Dai and D. Yu, *Energ. Environ. Sci.,* 2017, **10**, 893-899.
38 Oh, H. Y. Kim, H. Baik, B. Kim, N. K. Chaudhari, S. H. Joo and K. Lee, *Adv. Mater.,* 2019, **31**, 1805546.
39 X. Wang, P. Sun, H. Lu, K. Tang, Q. Li, C. Wang, Z. Mao, T. Ali and C. Yan, *Small*, 2019, **15**, 1804886.
40 Z. Yang, C. Zhao, Y. Qu, H. Zhou, F. Zhou, J. Wang, Y. Wu and Y. Li, *Adv. Mater.,* 2019, **31**, 1808043.
41 X. F. Lu, L. F. Gu, J. W. Wang, J. X. Wu, P. Q. Liao and G. R. Li, *Adv. Mater.,* 2017, **29**. 1604437
42 Y. Niu, W. Li, X. Wu, B. Feng, Y. Yu, W. Hu and C. M. Li, *J. Mater. Chem. A*, 2019, **7**, 10534-10542
43 X. Hu, S. Zhang, J. Sun, L. Yu, X. Qian, R. Hu, Y. Wang, H. Zhao and J. Zhu, *Nano Energy*, 2019, **56**, 109-117.
44 W. Shao, Y. Xia, X. Luo, L. Bai, J. Zhang, G. Sun, C. Xie, X. Zhang, W. Yan and Y. Xie, *Nano Energy*, 2018, **50**, 717-722.
45 L. Wang, Q. Zhou, Z. Pu, Q. Zhang, X. Mu, H. Jing, S. Liu, C. Chen and S. Mu, *Nano Energy*, 2018, **53**, 270-276.
46 Y. Zhao, J. Zhang, W. Wu, X. Guo, P. Xiong, H. Liu and G. Wang, *Nano Energy*, 2018, **54**, 129-137.
47 H. Huang, C. Yu, H. Huang, C. Zhao, B. Qiu, X. Yao, S. Li, X. Han, W. Guo, L. Dai and J. Qiu, *Nano Energy*, 2019, **58**, 778-785.

48 Q. Liang, L. Zhong, C. Du, Y. Luo, Y. Zheng, S. Li and Q. Yan, *Nano Energy*, 2018, **47**, 257-265.
49 H. Qiao, J. Yong, X. Dai, X. Zhang, Y. Ma, M. Liu, X. Luan, J. Cai, Y. Yang, H. Zhao and X. Huang, *J. Mater. Chem. A*, 2017, **5**, 21320-21327.
50 D.-J. Li, Z.-G. Gu, W. Zhang, Y. Kang and J. Zhang, *J. Mater. Chem. A*, 2017, **5**, 20126-20130.
51 S. Zhao, Y. Wang, J. Dong, C.-T. He, H. Yin, P. An, K. Zhao, X. Zhang, C. Gao, L. Zhang, J. Lv, J. Wang, J. Zhang, A. M. Khattak, N. A. Khan, Z. Wei, J. Zhang, S. Liu, H. Zhao and Z. Tang, Nature Energy, 2016, **1**, 16184
52 C. Guan, X. Liu, A. M. Elshahawy, H. Zhang, H. Wu, S. J. Pennycook and J. Wang, Nanoscale Horiz., 2017, **2**, 342-348.
53 X. Zhang, L. Huang, Q. Wang and S. Dong, *J. Mater. Chem. A*, 2017, **5**, 18839-18844.
54 J. Duan, S. Chen and C. Zhao, *Nat. Commun.,* 2017, **8**, 15341.
55 J. Luo, J.-H. Im, M. T. Mayer, M. Schreier, M. K. Nazeeruddin, N.-G. Park, S. D. Tilley, H. J. Fan and M. Grätzel, *Science*, 2014, **345**, 1593-1596.
56 C. Tang, N. Cheng, Z. Pu, W. Xing and X. Sun, *Angew. Chem. Int. Edit.,* 2015, 54, 9351-9355.
57 T. Yoon and K. S. Kim, *Adv. Funct. Mater.,* 2016, **26**, 7386-7393.
58 G.-F. Chen, T. Y. Ma, Z.-Q. Liu, N. Li, Y.-Z. Su, K. Davey and S.-Z. Qiao, *Adv. Funct. Mater.,* 2016, **26**, 3314-3323.
59 T. An, Y. Wang, J. Tang, W. Wei, X. Cui, A. M. Alenizi, L. Zhang and G. Zheng, *J. Mater. Chem. A*, 2016, **4**, 13439-13443.
60 Y.-Y. Chen, Y. Zhang, X. Zhang, T. Tang, H. Luo, S. Niu, Z.-H. Dai, L.-J. Wan and J.-S. Hu, *Adv. Mater.,* 2017, **29**, 1703311.
61 H. Liang, A. N. Gandi, D. H. Anjum, X. Wang, U. Schwingenschlogl and H. N. Alshareef, Nano Lett., 2016, **16**, 7718-7725.